ARTICLES
https://doi.org/10.1038/s41563-019-0396-2
nature materials

A map of the inorganic ternary metal nitrides

Wenhao Sun[1*], Christopher J. Bartel[2], Elisabetta Arca[3], Sage R. Bauers[3], Bethany Matthews[4], Bernardo Orvañanos[5], Bor-Rong Chen[6], Michael F. Toney[6], Laura T. Schelhas[6], William Tumas[3], Janet Tate[4], Andriy Zakutayev[3], Stephan Lany[3], Aaron M. Holder[2,3*] and Gerbrand Ceder[1,7]

Exploratory synthesis in new chemical spaces is the essence of solid-state chemistry. However, uncharted chemical spaces can be difficult to navigate, especially when materials synthesis is challenging. Nitrides represent one such space, where stringent synthesis constraints have limited the exploration of this important class of functional materials. Here, we employ a suite of computational materials discovery and informatics tools to construct a large stability map of the inorganic ternary metal nitrides. Our map clusters the ternary nitrides into chemical families with distinct stability and metastability, and highlights hundreds of promising new ternary nitride spaces for experimental investigation—from which we experimentally realized seven new Zn- and Mg-based ternary nitrides. By extracting the mixed metallicity, ionicity and covalency of solid-state bonding from the density functional theory (DFT)-computed electron density, we reveal the complex interplay between chemistry, composition and electronic structure in governing large-scale stability trends in ternary nitride materials.

Nitrides are an exciting space for materials design[1–3], as exemplified by state-of-the-art nitride materials for solid-state lighting[4,5], ceramic hard coatings[6], ammonia-synthesis catalysts[7], permanent magnets[8], superconductors[9], electrides[10,11], topological materials[12] and more. The nitride (N^{3-}) anion imparts unique electronic and bonding characteristics that are difficult to achieve in other chemical spaces, leading to useful optoelectronic and defect-tolerance properties[13] as well as strong metal–nitrogen bonds for structural stability and mechanical stiffness[14]. Despite much promise in the functionality of nitride materials, the nitrides remain relatively unexplored, with fewer than 400 unique ternary metal nitrides catalogued in the Inorganic Crystal Structure Database (ICSD), in contrast to over 4,000 ternary metal oxides. The paucity of known nitrides can largely be attributed to the challenging requirements of nitride synthesis. Because the N_2 molecule is so stable, solid-state nitrides generally have small formation energies; they decompose at high temperature; and they must be synthesized in oxygen- and water-free atmospheres to achieve high purity[2,15,16]. These stringent synthesis constraints, coupled with the poor intrinsic stabilities of nitrides, impose considerable risk on the exploratory synthesis of nitride materials.

High-throughput computational materials science has emerged as a new paradigm for materials discovery[17,18], helping to guide experimental synthesis efforts across broad and uncharted chemical spaces[19,20]. Here, we employ a suite of computational materials discovery[21,22] and informatics[23,24] tools to survey, visualize and explain stability relationships across the inorganic ternary metal nitrides. Our investigation proceeds in three steps. First, we use crystal-structure prediction algorithms to probe the stability landscapes of previously unexplored ternary nitride spaces, identifying hundreds of promising new ternary nitrides for further exploratory synthesis. Guided by these predictions, we successfully synthesize seven new Zn- and Mg-based ternary nitrides. Next, we use unsupervised machine-learning algorithms to cluster together cations with a similar propensity to form stable or metastable ternary nitrides. To visualize these clustered nitride families, we construct a large and comprehensive stability map of the inorganic ternary metal nitrides. Our map reveals broad overarching relationships between nitride chemistry and thermodynamic stability, and inspires us to rationalize these trends from their underlying chemical origins[25]. To do so, we extract from the DFT-computed electron density the mixed metallicity, ionicity and covalency of solid-state bonding, which we use to formulate data-driven insights into the thermochemical and electronic origins of ternary nitride stability.

Beyond the nitrides, there remain many other unexplored chemical spaces awaiting experimental discovery. Our computational approach here can be further applied to these uncharted chemical spaces, not only to predict and synthesize new compounds, but also to visualize general trends over broad compositional spaces—providing maps and chemical intuition to help experimental chemists navigate exploratory synthesis at the frontier of solid-state chemistry.

Nitride chemistry and thermodynamic stability

In this work, we explore ternary nitrides over a 50×50 M_1–M_2–N composition space, where M consists of the 50 most common cations in the known nitrides: spanning over the alkali, alkaline-earth, transition, precious and post-transition metals, as well as the main-group elements B, C, Si, S and Se. Within this composition matrix, known ternary nitrides are found over only 307 M_1–M_2–N spaces. To fill in the missing spaces, we first conduct a high-throughput computational search for new ternary nitride compounds. Previous computational searches for ternary nitrides have been constrained to either limited composition spaces[26,27] or specific crystal structures[28,29]. Here, we broadly sample over both composition and crystal structure, using a data-mined structure predictor (DMSP)[30] to perform statistically probable chemical substitutions on the known ternary nitrides, generating new but reasonable candidate ternary nitride phases in silico.

[1]Materials Sciences Division, Lawrence Berkeley National Laboratory, Berkeley, CA, USA. [2]Department of Chemical and Biological Engineering, University of Colorado, Boulder, CO, USA. [3]National Renewable Energy Laboratory, Golden, CO, USA. [4]Department of Physics, Oregon State University, Corvallis, OR, USA. [5]Department of Materials Science and Engineering, Massachusetts Institute of Technology, Cambridge, MA, USA. [6]SLAC National Accelerator Laboratory, Menlo Park, CA, USA. [7]Department of Materials Science and Engineering, UC Berkeley, Berkeley, CA, USA. *e-mail: wenhaosun@lbl.gov; Aaron.Holder@colorado.edu

Table 1 | Statistics of the known and predicted ternary metal nitrides, categorized by the thermodynamic stability of ternary M_1–M_2–N spaces, and specific ternary $A_xB_yN_z$ phases within these spaces. All spaces are categorized by the ΔH_f of the ternary nitride with the lowest formation energy. Metastable phases are categorized by their energy above the convex hull, ΔE_{hull}

Ternary M_1–M_2–N spaces	Previously known	Newly predicted	Portion of map
Systems with stable ternary nitrides (blue)	200	93	293 (30%)
- *Stable alkali–metal–nitride systems*	*128*	*76*	*204*
- *Stable metal–metal–nitride systems*	*72*	*17*	*89*
Metastable versus stable binaries, $\Delta H_f < 0$ (green)	88	322	410 (43%)
Metastable versus elements, $\Delta H_f > 0$ (red)	19	241	260 (27%)
Metastable: stabilizable with $\Delta\mu_N < +1$ eV per N	0	63	63
Metastable: stabilizable with pressure ≥ 1 GPa	13	86	99
Ternary $A_xB_yN_z$ phases	**Previously known**	**Newly predicted**	**Total number**
Stable ternary phases	213	244	447
Metastable, $\Delta E_{hull} < 70$ meV per atom	92	417	509
Metastable, $\Delta E_{hull} < 200$ meV per atom	118	1,213	1,331
Metastable: stabilizable with $\Delta\mu_N < +1$ eV per N	3	92	95
Metastable: stabilizable with pressure ≥ 1 GPa	99	348	447

Previously, we trained a DMSP algorithm specifically for nitride discovery (Methods)[31]; we use it here to extrapolate the 340 known ternary nitrides (213 stable + 127 metastable) to 6,000 hypothetical ternary nitride structures, surveyed over 963 ternary M_1–M_2–N spaces. We evaluate the phase stability of these DMSP-generated nitrides using ab initio thermodynamics, leveraging the tools and precomputed data from the Materials Project database (Methods)[32,33]. Our results are summarized in Table 1. Notably, we predict 244 new stable ternary nitride compounds, more than doubling the 213 previously known stable ternary nitrides. These stable ternary nitrides span 293 ternary M_1–M_2–N spaces, 93 of which were not previously known to contain any stable ternary nitrides. A small subset of these stable ternary nitrides were identified in previous computational searches (refs. [26–29] and Supplementary Section 1) and have been reconfirmed here.

Permuting chemistry and crystal structure on the known ternary nitrides provides a computationally efficient probe of formation energies over broad ternary nitride compositions. One limitation of the DMSP is that, because it operates by chemical substitution, if the structural prototype of a ground-state nitride has never been observed before, then the DMSP cannot predict it. Nevertheless, because most ternary nitride spaces are unexplored, the prediction of any ternary nitride structure with negative formation energy in an otherwise empty chemical space implies that the true ground-state structures and compositions must be even lower in energy—thereby highlighting that ternary space as a compelling target for further theoretical and experimental investigations.

A stability map of the ternary metal nitrides

A long list of predicted compounds can be difficult to navigate, and does not provide an intuitive picture of the structural form of a chemical space. Similar to how Mendeleev's periodic table revealed the underlying structure of the elements, an effective visual organization can reveal hidden relationships and chemical families within the ternary metal nitrides. Here, we elucidate the structural form[34] of the ternary nitride space using hierarchical agglomeration[35]—which is an unsupervised machine-learning algorithm—to cluster together metals with a similar propensity to form either stable or metastable ternary nitrides. To capture both large-scale stability trends and local chemical relationships, we build a multifeature distance metric that considers for each ternary nitride its formation energy, whether it is stable or metastable, and the periodic group in which the metal lies. These multiple features represent mixed data types (continuous, nominal and ordinal, respectively), which we combine into a single distance metric using Gower's method (Methods)[36].

The agglomeration algorithm clusters elements hierarchically by minimizing this multifeature distance matrix. The resulting dendrogram provides a phenotypic representation of the nitride chemical families, and results in a corresponding one-dimensional ordering of the metal cations. In the spirit of Pettifor's phenomenological structure maps[37], we use this one-dimensional elemental ordering to construct a clustered heatmap of the ternary metal nitrides, shown in Fig. 1, coloured to represent the stability of the ternary metal nitride with the lowest formation energy in each M_1–M_2–N chemical space. Our clustering algorithm parses the ternary nitrides map into distinct regions of stability (blue), metastability against binaries (green) and metastability against elements (red)—highlighting stable ternary nitride spaces that are promising for further exploratory synthesis, and metastable spaces where successful synthesis may require non-equilibrium synthesis routes. An interactive version of the map, with ternary phase diagrams and compound stability information for each M_1–M_2–N system, is available in Supplementary Section 3.

Stable ternary nitrides

Thermodynamically stable ternary nitrides comprise less than a third of the map, which is probably a confounding factor in the difficulty of ternary nitride discovery. Alkali and alkaline-earth ternary metal nitrides (Alk–Me–N) represent a majority of the stable spaces (200/293 = 68%), whereas stable non-alkali metal–metal nitrides (Me–Me–N) are less common, with small islands of stability scattered amongst the mixed transition- and precious-metal nitrides.

Our clustering algorithm distinguishes between three major groups of alkali/alkaline-earth metals in their ability to form ternary nitrides. The first group—Li, Ca, Sr and Ba—reacts with all elements to form ternary nitrides with negative formation enthalpy, ΔH_f, most of which are thermodynamically stable. Na, K, Rb and Cs form stable ternaries with early and first-row transition metals, although they often react unfavourably ($\Delta H_f > 0$) with precious metals and metalloids. The clustering algorithm places Mg and Zn as intermediate between these two groups: Mg is less reactive than the other alkaline earth metals—forming ternaries less exothermically and forming fewer stable ternary nitrides overall; while Zn is a

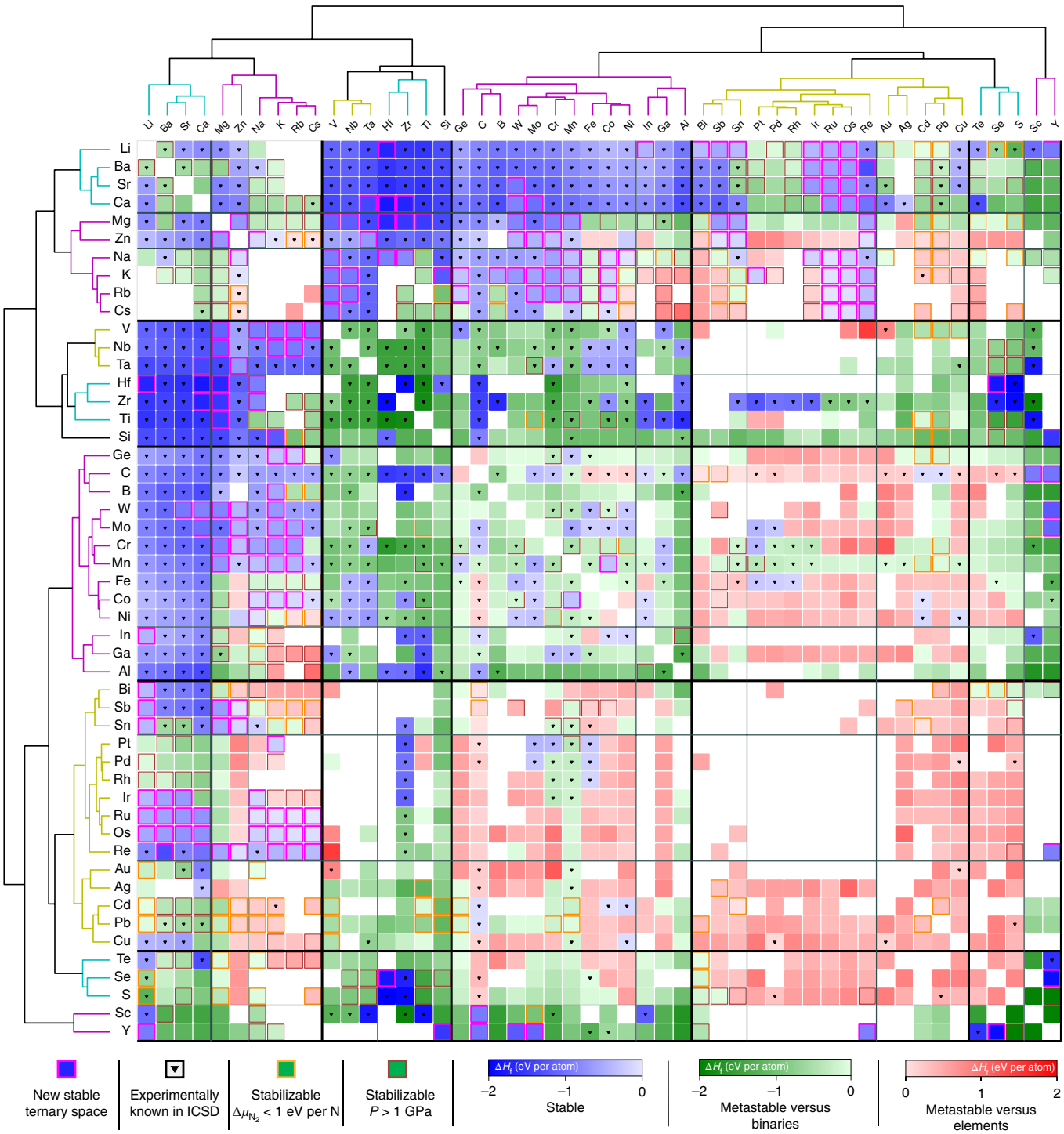

Fig. 1 | A map of the inorganic ternary metal nitrides, coloured to represent the thermodynamic stability of the ternary nitride with the lowest formation energy. Blue: stable ternary nitrides on the convex hull. Green: ternaries with $\Delta H_f < 0$ but metastable with respect to binaries. Red: ternaries metastable with respect to elements, $\Delta H_f > 0$. Triangles represent ternary nitride systems with entries in the ICSD. White spaces indicate that the DMSP did not find probable chemical substitutions to create a structure in that system. Elements are clustered on multiple features to indicate their propensity to form stable or metastable ternary nitrides. These clustered elements are represented phenotypically by a dendrogram, which parses the ternary nitrides map into regions of distinct stability and metastability. An interactive version of the ternary nitrides map, with phase diagrams and compound stability information for each ternary system, is available in Supplementary Section 3.

relatively electropositive transition metal that can react like an alkali ion when coupled with early transition metals.

Of the 293 spaces with stable ternary nitrides, the 93 indicated on the map by a magenta box do not have any ternary nitride entries in the current ICSD, and therefore represent predictions in this work. Our search identifies many new stable ternary nitrides containing Na, K, Rb, Cs, Mg and Zn, as well as several new ternary Sc and Y nitrides. Interestingly, Ir, Ru, Re and Os are found to form stable

ternary nitrides when combined with most alkali and alkaline-earth metals. We eagerly await the experimental discovery of these newly predicted families of stable ternary nitrides.

Metastable ternary nitrides

Ternary nitrides that are metastable against decomposition into binary phases (green) or elemental phases (red) comprise a majority of the surveyed spaces. Although metastable nitrides should, in principle, be difficult to synthesize, ternary nitrides have been experimentally realized in 107 of the computed metastable spaces, shown in Fig. 1 by the inverted triangles. Indeed, we previously found nitrides to be the most metastable class of chemical compounds—having the largest fraction of metastable phases, as well as the highest average energies above the ground-state phases[38,39]. The unusual metastability of nitrides can be attributed to the cohesivity afforded by strong metal–nitrogen bonds in the solid state, which can kinetically 'lock in' metastable nitride structures.

By formulating rational synthesis strategies for these metastable nitrides, we can expand the design space of functional nitride materials beyond equilibrium phases and compositions. One thermodynamic route to metastable nitrides is through nitrogen precursors that are less strongly bound than triple-bonded N_2[13,31], such as ammonia[15], azides[40] or plasma-cracked N_2[41]. Recently, we showed that plasma-cracked atomic N precursors can reach nitrogen chemical potentials of $\Delta\mu_N \approx +1$ eV per N, which can be used to sputter remarkably metastable nitride thin films, such as $SnTi_2N_4$ (metastable by 200 meV per atom)[42], or $ZnMoN_2$ in a wurtzite-derived structure (metastable by 160 meV per atom)[43]. High-pressure synthesis is another potent route to dense and nitrogen-rich metastable nitrides[44]. Using the method of Amsler et al.[45], we further computed the stability of the DMSP-suggested ternary nitrides under elevated pressures and supercritical N_2 fugacity[43] (Methods). In Fig. 1, we use orange boxes to highlight 63 spaces with metastable ternary nitrides stabilizable under $\Delta\mu_N < +1$ eV per N, and brown boxes to highlight 99 spaces with metastable ternary nitrides that are stabilizable under pressures of 1 GPa or more.

Metastable ternary nitrides are also accessible through soft solid-state synthesis routes; for example, delafossite $CuTaN_2$ is metastable by 127 meV per atom, but can be synthesized by ion exchange of Cu^+ for Na^+ from the stable $NaTaN_2$ phase[46]. Amorphous phases can also be a route to metastable ternary nitrides, whereby an atomically homogeneous amorphous ternary nitride precursor is gently annealed to a lower-energy, but still metastable, target crystalline phase[47,48]. Decomposition of metastable ternary nitrides can also drive interesting functionality; for example, phase segregation of metastable Si–Ti–N alloys at high temperature leads to complex TiN/Si_3N_4 layered heterostructures with superior mechanical properties for tribological applications[6].

Validation of predicted ternary nitrides

Ternary II–IV nitrides (where II = Mg, Zn and IV = Si, Ge, Sn) have recently emerged as compelling semiconducting materials, due to their chemical similarity to III–N semiconductors[26,49]. Here, we explore new Zn- and Mg-based ternary nitrides with transition-metal (TM) elements, targeting seven previously unexplored II–TM–N spaces for deeper investigation: Zn–Mo–N, Zn–W–N, Zn–Sb–N, Mg–Ti–N, Mg–Zr–N, Mg–Hf–N and Mg–Nb–N. Following the broad DMSP stability screening, we next use kinetically limited minimization[43] to conduct a full unconstrained ground-state crystal-structure search in these seven spaces (Methods). We tabulate the resulting crystal structures and formation energies in Table 2.

As illustrated in Fig. 2a, we predict Zn-based ternary nitrides to crystallize in a wurtzite-derived structure, and Mg-based ternaries to form in a rocksalt-derived structure. Using magnetron sputtering, we successfully synthesized crystalline ternary nitride thin films in all seven II–TM–N spaces. Figure 2b shows synchrotron X-ray diffraction (XRD) patterns of these synthesized nitrides. The experimental XRD patterns match the peak positions and intensities of reference patterns for rocksalt and wurtzite prototypes well, with small differences in relative intensities arising from the textured growth of the thin films, as well as different scattering powers within the unit cell. Notably, we do not observe peak-splitting relative to the ideal wurtzite or rocksalt structures, suggesting disorder on the cation sites, which may provide an interesting avenue to tune electronic properties[50]. See Methods and Supplementary Section 4 for further details of structure prediction, synthesis and characterization. We report the semiconducting properties of these new II–TM–N materials in separate publications.

Table 2 | Seven new Zn- and Mg-based ternary nitrides with structures predicted by unconstrained crystal-structure search, and their respective formation energies

Wurtzite derived	Pred. space group	ΔH_f (eV per atom)
Zn_2SbN_3	$Cmc2_1$ (no. 36)	−0.037
Zn_3WN_4	$Pmn2_1$ (no. 31)	−0.437
Zn_3MoN_4	$Pmn2_1$ (no. 31)	−0.367
Rocksalt derived	**Pred. space group**	**ΔH_f (eV per atom)**
Mg_2NbN_3	$C2/m$ (no. 12)	−1.175
$MgHfN_2$	$I4_1/amd$ (no. 141)	−1.662
$MgZrN_2$	$I4_1/amd$ (no. 141)	−1.521
$MgTiN_2$	$R\bar{3}m$ (no. 166)	−1.479

Historically, the rate of discovering new ternary nitride M_1–M_2–N spaces has averaged about 3.3 per year, as illustrated in Fig. 2c. Our rapid experimental realization of ternary nitrides in seven previously unexplored M_1–M_2–N spaces validates the predictions from the map, bolsters confidence in the 86 other predicted spaces with stable nitrides and highlights the valuable role of computational materials discovery in accelerating exploratory synthesis in new chemical spaces.

Origins of ternary nitride stability

Understanding why certain metals react favourably to form stable ternary nitrides, whereas others do not, is a fundamental question that probes at the very heart of solid-state chemistry. We can achieve some insights towards this question by considering the geometric requirements of thermodynamic stability. A ternary nitride is stable if it is lower in free energy than any stoichiometric combination of its competing ternaries, binaries or elemental constituents. In formation-energy versus composition space, this stability requirement manifests geometrically as a convex hull, illustrated for a ternary A–B–N space in Fig. 3a. We can therefore rationalize the stability of a ternary nitride from (1) a thermochemical perspective—if a ternary nitride is lower in energy than its competing binary nitrides—and (2) a solid-state bonding perspective—how two metals interact electronically within a ternary nitride to raise or lower the bulk lattice energy of the ternary compound.

Thermochemical decomposition into competing binaries. To quantify the thermochemical propensity of a ternary nitride to decompose into its competing binaries, we first define a feature named the 'depth of the binary hull', referring to the lowest-energy binary nitride in a binary Me–N space. This binary-hull depth, illustrated in Fig. 3a by a black dashed line, serves as a proxy for the strength of the pairwise metal–nitrogen bond in the solid state. Figure 3b shows for each element the number of stable ternary spaces in which it forms versus the depth of the binary hull. A volcano plot emerges, where elements that have either shallow

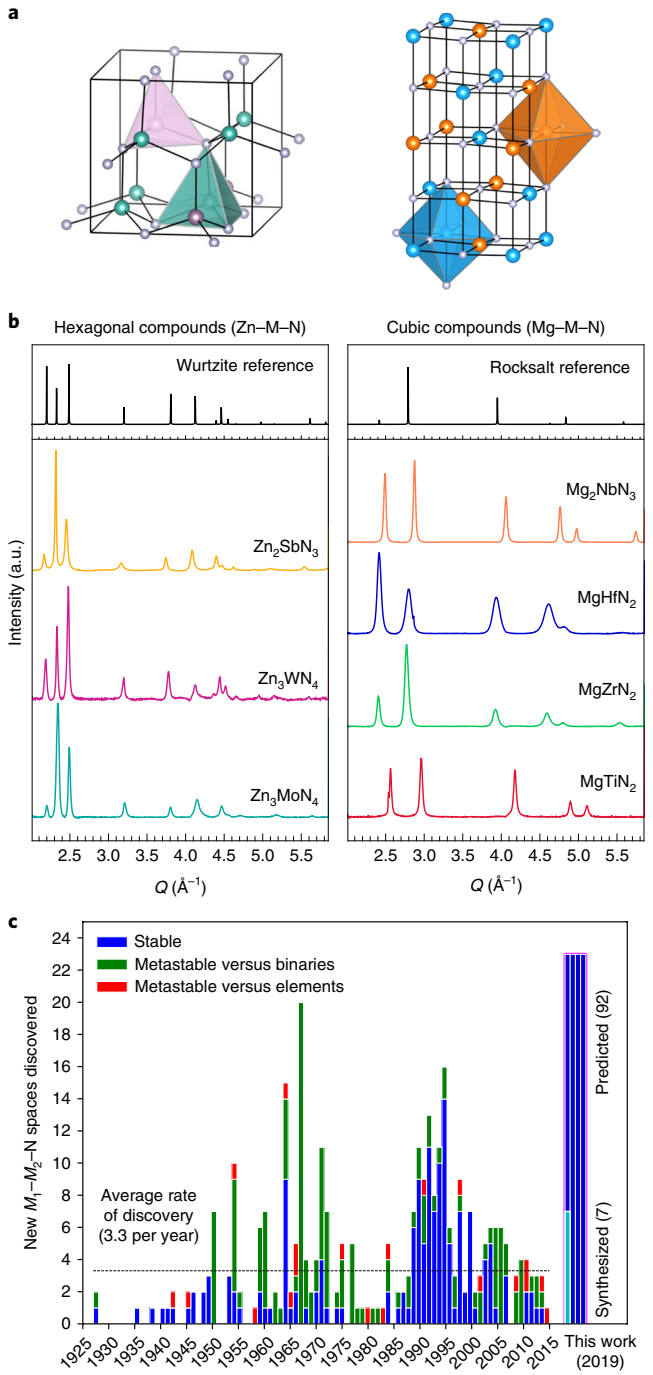

Fig. 2 | Experimental realization of seven predicted Zn- and Mg-based ternary nitrides. a, Zn-based ternary nitrides form in a wurtzite-derived structure (left), and Mg-based ternary nitrides crystallize in a rocksalt-derived structure (right). **b**, Synchrotron-measured XRD patterns of new Zn- and Mg-based ternary nitrides, shown with reference diffraction patterns for rocksalt (NaCl) and wurtzite (ZnS), adjusted to lattice parameters of $a = 4.5$ Å and $a = 3.3$ Å/$c = 5.4$ Å to approximate the average peak positions in the experimental patterns. Q is related to diffraction angle (θ) and incident wavelength (λ) by $Q = (4\pi/\lambda)\sin(\theta)$ and $\lambda = 0.9744$ Å. **c**, Discovery histogram for new ternary nitride spaces, based on entries as catalogued in the ICSD. A table of discovery dates is given in Supplementary Section 5.

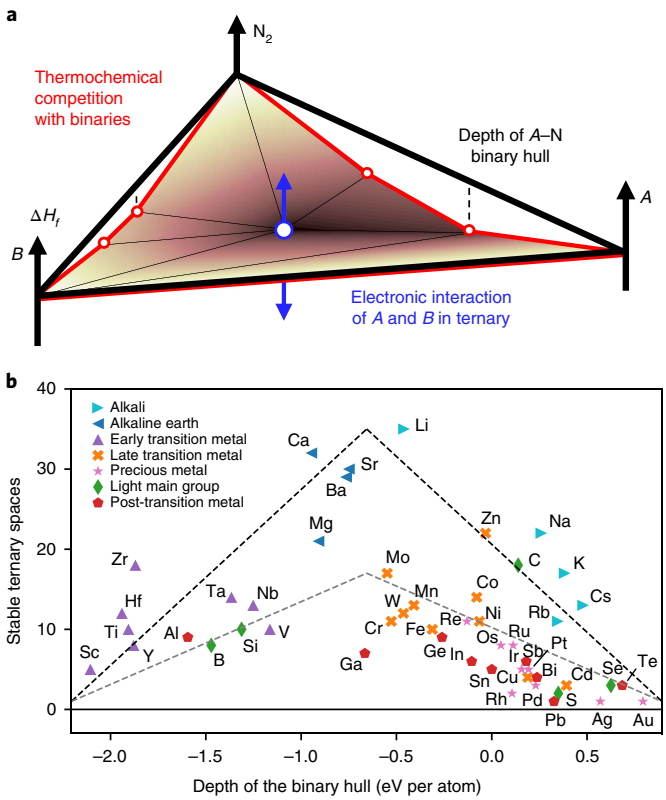

Fig. 3 | Thermochemical origins of ternary nitride stability. a, Convex hull of a ternary A–B–N system, where the vertical axis is formation energy and the horizontal triangular plane is composition. The stability of a ternary nitride (blue circle) is governed by its propensity to decompose into competing binaries (red lines), as well as by its lattice energy arising from the electronic interaction of two metals in the ternary nitride (blue arrows). **b**, Scatterplot showing the number of stable ternary nitride spaces in which each metal appears, plotted against the depth of the binary hull, which corresponds to the binary nitride with lowest formation energy in the Me–N binary space. The deepest-hull binaries and their formation energies are listed in Supplementary Section 6. In some binary nitride spaces, the binary nitride with the lowest formation energy has positive formation energy, such as Cu_3N in the Cu–N hull, indicating that Cu_3N decomposes to Cu(s) + N_2(g) under ambient conditions. Dashed lines provide guides for the eye for the volcano trend.

or deep binary nitride hulls tend not to form many stable ternary nitrides, whereas elements that have intermediate binary-nitride-hull depths (around −0.8 eV per atom) form stable ternary nitrides most readily. From a thermochemical perspective, when the binary hull is deep there is a greater propensity for a ternary metal nitride to phase-separate into its competing low-energy binary nitrides. On the other hand, a shallow (or positive) binary-hull depth indicates intrinsically weak metal–nitrogen bonding, meaning that nitride formation is probably unfavourable in the first place. Intermediate binary-hull depths provide favourable metal–nitrogen bonding, but not enough for decomposition of a ternary nitride into its binary constituents—offering a compromise between these two competing effects.

Electronic origins of ternary nitride stability. Alkali and alkaline-earth metals stand out on the volcano in Fig. 3b, forming stable ternaries more readily than other elements with similar binary-hull depths. Qualitatively, we expect differences in the electronegativity between A, B and N to redistribute the electron density into different bonds, which in the solid state may have mixed metallic, ionic and covalent character. In the Methods, we describe new semiquantitative schemes to extract the metallicity[51], ionicity[52] and covalency[25]

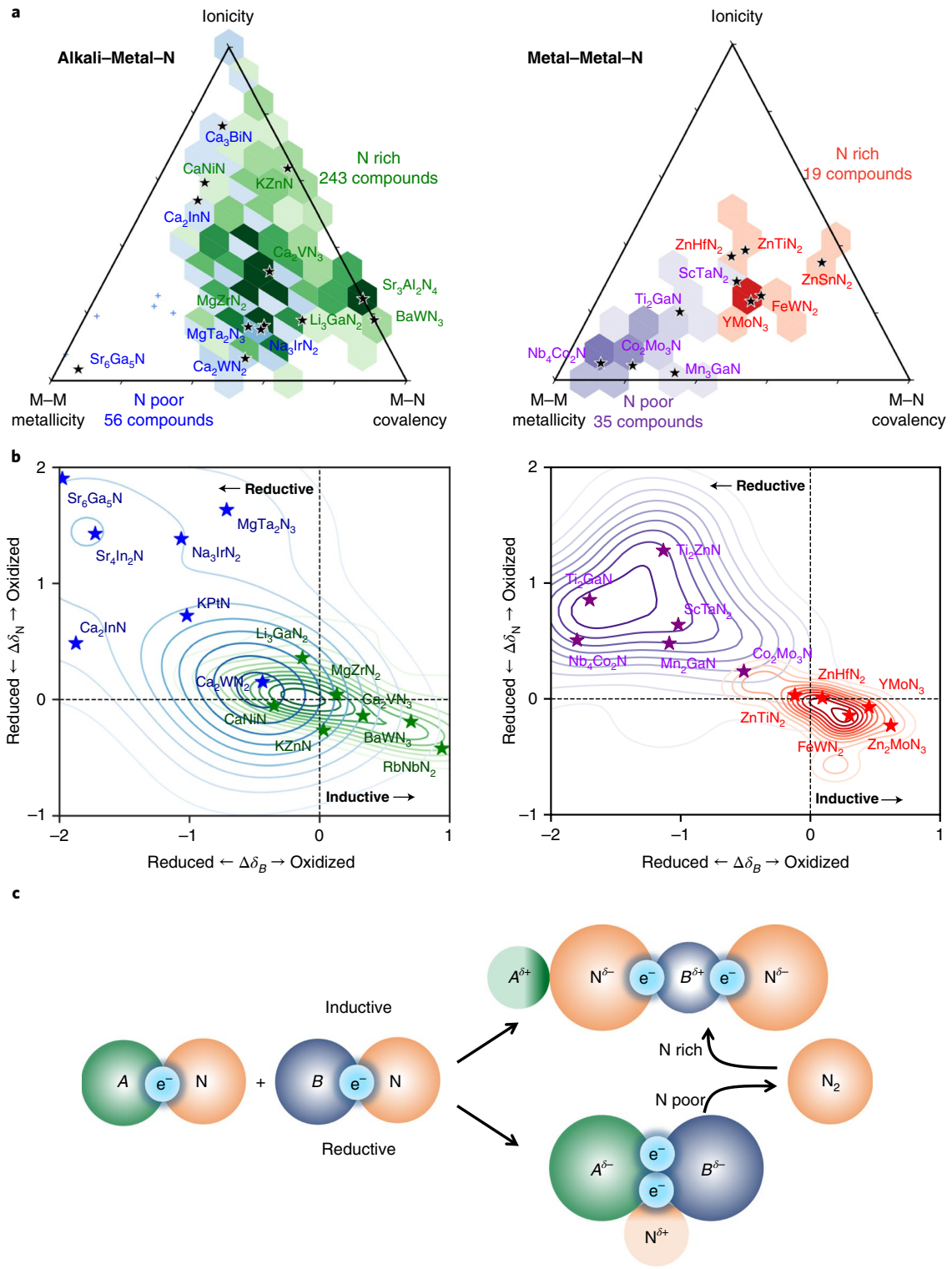

Fig. 4 | Electronic structure origins of ternary nitride stability. a, Metallicity, ionicity and covalency of the stable ternary nitrides, hexagonally binned on van Arkel triangles by the nitrogen excess or nitrogen deficiency of the ternary, compositionally referenced against the deepest-hull binary nitrides. Hexagons are plotted for regions with more then two data points only; outliers are shown with small crosses. The colour intensity corresponds to the number density in each hexagon. Full van Arkel scatter plots can be found in Supplementary Section 8. **b**, Kernel density distributions of ion oxidation and reduction between the deepest-hull binary nitrides and the stable ternary nitride, as determined from the DFT-computed charge density, for the nitrogen anion (vertical axis) and the more electronegative metal, *B* (horizontal axis). **c**, Inductive effect: electropositive metal *A* donates electron density to the *B*–N covalent bond, oxidizing the more electronegative metal, which can lead to nitrogen-rich nitrides. Reductive effect: nitrogen oxidation or nitrogen release provides electrons to Me–Me bonds, reducing the metals and increasing metallicity.

from the DFT-computed electron density. We plot this mixed solid-state bonding character for stable ternary nitrides in Fig. 4a, on the classic metallic–ionic–covalent axes of van Arkel triangles[53].

From Fig. 4a, we see that stable Alk–Me–N ternaries tend to exhibit greater ionicity and metal–nitrogen covalency, whereas stable Me–Me–N ternaries generally have higher metallicity. This distinction becomes even more apparent when the triangles are further separated into nitrogen-rich and nitrogen-poor nitrides, where this nitrogen excess or deficiency is compositionally referenced against the deepest-hull binary nitrides. Stable Alk–Me–N ternaries are mostly nitrogen rich, whereas most stable Me–Me–N ternaries are nitrogen poor. This dichotomy between nitrogen-rich and nitrogen-poor ternary nitrides can largely be understood by how electron density redistributes between the nitrogen anion and the more electronegative metal during a reaction from the deepest-hull binary nitrides to a ternary nitride. Figure 4b plots the changes in ionicity of the nitrogen anion, $\Delta\delta_N$, and the more electronegative metal cation, $\Delta\delta_B$, during such a reaction. These changes in ionicity are proxies for ion oxidation and reduction, measured relative to the *B* or N ions as they exist in the corresponding deepest-hull binary nitrides (Methods).

The formation of nitrogen-rich nitrides can be rationalized primarily from the inductive effect[1,54], where an electropositive metal, *A*, donates electron density to its adjacent nitrogen anion, driving the formation of strong nitrogen covalent bonds with the more electronegative metal, *B*. As illustrated in Fig. 4b,c, this electron donation from *A* generally leads to nitrogen reduction, which in turn oxidizes the metal *B*. Extensive oxidation of *B* can be compensated by excess nitrogen—explaining the formation of nitrogen-rich nitrides. An oxidized cation and reduced anion increases the overall ionicity of the $A^{\delta+}[B\text{–}N]^{\delta-}$ framework, resulting in nitride ceramics with very negative electrostatic Madelung energies. Because alkali and alkaline-earth metals are so electropositive, the inductive effect drives the strong exothermic formation energies of Alk–Me–N ternaries, explaining their predominance within the ternary nitride map. The inductive effect can also be operative in nitrogen-rich Me–Me–N: most frequently with Zn, which is a relatively electropositive transition metal and often acts as an electron donor—a fact empirically captured by the hierarchical clustering algorithm.

For stable nitrogen-poor nitrides, we propose a new mechanism named the reductive effect, where remarkably the nitrogen anion can also serve as an electron donor for metal reduction. For some ternary Me–Me–N compositions, Me–Me bonds may be stronger than Me–N bonds. As shown in Fig. 4c, the oxidation or release of electrophilic nitrogen anions (relative to the deepest-hull binaries) can redistribute electron density back to these strong Me–Me bonds, reducing the corresponding metals. The reductive effect can stabilize carbide-like structures, for example in Co_2Mo_3N, which exhibits infinite one-dimensional chains of covalently bonded $[Co\text{–}Co]_\infty$ intertwined within an extended Mo–N covalent network (structure in Supplementary Section 9). The reductive effect can also be operative in stable nitrogen-poor stoichiometries of Alk–Me–N compounds, such as $Sr_3Ge_2N_2$, which features unusual infinite one-dimensional $[Ge\text{–}Ge]^{2-}_\infty$ chains throughout an otherwise ionic $(Sr^{2+})_2[GeN_2]^{4-}$ lattice (structure in Supplementary Section 9). The data-mining structure prediction algorithm used in this work operates on ionic substitution, which may not be ideally poised to predict nitrogen-poor nitrides due to their ambiguous valence states, suggesting that there may still be many Me–Me–N ternary nitrides stabilized by the reductive effect awaiting prediction.

Our analysis demonstrates that the nitrogen anion can be fairly amphoteric in the solid state—usually acting as an electron acceptor under the inductive effect to form oxide-like ionic/covalent nitride ceramics, but sometimes serving as an electron donor in the reductive effect, driving the formation of carbide-like metallic subnitrides. The span of electronic structures available to the ternary nitrides offers a rich design space for materials functionality. Incorporating an alkali metal into an otherwise metallic binary nitride can increase charge localization driven by the inductive effect, opening a bandgap for functional semiconducting nitrides suitable for solid-state lighting, piezoelectrics, photovoltaic energy conversion and more. On the other hand, nitrogen-poor nitrides possess metallic bonding punctuated by charge localization on nitrogen atoms, which can lead to complex electronic and magnetic structures, and may serve as the basis for new superconductors, permanent magnets and topological materials. Modifying the nitrogen stoichiometry within a chemical space can be an effective strategy to compositionally tune the electronic structure between the reductive and inductive effects. For example, varying the Zn/Mo ratio in a wurtzite-based Zn–Mo–N compound can modulate the molybdenum oxidation state from Mo^{4+} to Mo^{6+}, turning conductive $ZnMoN_2$ into insulating Zn_3MoN_4, a wide-bandgap semiconductor[43].

Outlook

The library of inorganic solids has been dominated by oxides, whose structures and chemistries are often known from mineralogy. Compounds that do not form readily under ambient conditions, such as nitrides, offer a new frontier for materials discovery and design—so long as we have a rational understanding of the factors that drive stability in these relatively unexplored spaces. In this work, we used computational materials discovery and informatics tools to build a large stability map of the ternary nitrides space. Our objective was not only to predict and synthesize new ternary metal nitrides, but further to visualize large-scale relationships between nitride chemistry and thermodynamic stability, and to rationalize these trends from their deeper chemical origins. Our map as it stands is necessarily incomplete—it represents a current upper bound on the ternary nitride stability landscape. As new exotic structures and bonding motifs are discovered in the ternary metal nitrides, the procedures in this work can be iteratively reapplied to update and refine our understanding of this extended compositional space. From a broader perspective, our computational approach offers a systematic blueprint for mapping uncharted chemical spaces, providing synthetic chemists with guidance in their quest to continuously extend the frontier of solid-state chemistry.

Online content

Any methods, additional references, Nature Research reporting summaries, source data, statements of code and data availability and associated accession codes are available at https://doi.org/10.1038/s41563-019-0396-2.

Received: 14 September 2018; Accepted: 5 May 2019;
Published online: 17 June 2019

References

1. DiSalvo, F. J. & Clarke, S. J. Ternary nitrides: a rapidly growing class of new materials. *Curr. Opin. Solid State Mater. Sci.* **2**, 241–249 (1996).
2. Höhn, P. & Niewa, R. Nitrides of non-main group elements. *Handb. Solid State Chem.* **1**, 251–359 (2017).
3. Tareen, A. K., Priyanga, G. S., Behara, S., Thomas, T. & Yang, M. Mixed ternary transition metal nitrides: a comprehensive review of synthesis, electronic structure, and properties of engineering relevance. *Prog. Solid State Chem.* **53**, 1–26 (2018).
4. Amano, H., Kito, M., Hiramatsu, K. & Akasaki, I. P-type conduction in Mg-doped GaN treated with low-energy electron beam irradiation (LEEBI). *Jpn. J. Appl. Phys.* **28**, L2112–L2114 (1989).
5. Pust, P. et al. Narrow-band red-emitting $Sr[LiAl_3N_4]:Eu^{2+}$ as a next-generation LED-phosphor material. *Nat. Mater.* **13**, 891–896 (2014).
6. Vepřek, S. & Reiprich, S. A concept for the design of novel superhard coatings. *Thin Solid Films* **268**, 64–71 (1995).
7. Jacobsen, C. J. H. Novel class of ammonia synthesis catalysts. *Chem. Commun.* **2000**, 1057–1058 (2000).

8. Coey, J. & Sun, H. Improved magnetic properties by treatment of iron-based rare earth intermetallic compounds in ammonia. *J. Magn. Magn. Mater.* **87**, L251–L254 (1990).
9. Balbarin, V., Dover, R. V. & Disalvo, F. The high temperature preparation and property measurements of $CaTaN_2$: a ternary superconducting nitride. *J. Phys. Chem. Solids* **57**, 1919–1927 (1996).
10. Lee, K., Kim, S. W., Toda, Y., Matsuishi, S. & Hosono, H. Dicalcium nitride as a two-dimensional electride with an anionic electron layer. *Nature* **494**, 336–340 (2013).
11. Burton, L. A., Ricci, F., Chen, W., Rignanese, G.-M. & Hautier, G. High-throughput identification of electrides from all known inorganic materials. *Chem. Mater.* **30**, 7521–7526 (2018).
12. Huang, H., Jin, K.-H. & Liu, F. Alloy engineering of topological semimetal phase transition in $MgTa_2{-}xNb_xN_3$. *Phys. Rev. Lett.* **120**, 136403 (2018).
13. Zakutayev, A. Design of nitride semiconductors for solar energy conversion. *J. Mater. Chem. A* **4**, 6742–6754 (2016).
14. Mori-Sánchez, P. et al. Origin of the low compressibility in hard nitride spinels. *Phys. Rev. B* **68**, 064115 (2003).
15. Elder, S. H., Disalvo, F. J., Topor, L. & Navrotsky, A. Thermodynamics of ternary nitride formation by ammonolysis: application to lithium molybdenum nitride ($LiMoN_2$), sodium tungsten nitride (Na_3WN_3), and sodium tungsten oxide nitride (Na_3WO_3N). *Chem. Mater.* **5**, 1545–1553 (1993).
16. Mchale, J. M., Navrotsky, A., Kowach, G. R., Balbarin, V. E. & Disalvo, F. J. Energetics of ternary nitrides: Li–Ca–Zn–N and Ca–Ta–N systems. *Chem. Mater.* **9**, 1538–1546 (1997).
17. Curtarolo, S. et al. The high-throughput highway to computational materials design. *Nat. Mater.* **12**, 191–201 (2013).
18. Jain, A, Shin, Y. & Persson, K. A. Computational predictions of energy materials using density functional theory. *Nat. Rev. Mater.* **1**, 15004 (2016).
19. Collins, C. et al. Accelerated discovery of two crystal structure types in a complex inorganic phase field. *Nature* **546**, 280–284 (2017).
20. Gautier, R. et al. Prediction and accelerated laboratory discovery of previously unknown 18-electron ABX compounds. *Nat. Chem.* **7**, 308–316 (2015).
21. Hautier, G., Fischer, C. C., Jain, A., Mueller, T. & Ceder, G. Finding nature's missing ternary oxide compounds using machine learning and density functional theory. *Chem. Mater.* **22**, 3762–3767 (2010).
22. Meredig, B. et al. Combinatorial screening for new materials in unconstrained composition space with machine learning. *Phys. Rev. B* **89**, 094104 (2014).
23. Jain, A., Hautier, G., Ong, S. P. & Persson, K. New opportunities for materials informatics: resources and data mining techniques for uncovering hidden relationships. *J. Mater. Res.* **31**, 977–994 (2016).
24. Isayev, O. et al. Materials cartography: representing and mining materials space using structural and electronic fingerprints. *Chem. Mater.* **27**, 735–743 (2015).
25. Hoffmann, R. How chemistry and physics meet in the solid state. *Angew. Chem. Int. Ed.* **26**, 846–878 (1987).
26. Hinuma, Y. et al. Discovery of earth-abundant nitride semiconductors by computational screening and high-pressure synthesis. *Nat. Commun.* **7**, 11962 (2016).
27. Gharavi, M. A., Armiento, R., Alling, B. & Eklund, P. Theoretical study of phase stability, crystal and electronic structure of $MeMgN_2$ (Me = Ti, Zr, Hf) compounds. *J. Mater. Sci.* **53**, 4294–4305 (2018).
28. Ching, W. Y., Mo, S.-D., Tanaka, I. & Yoshiya, M. Prediction of spinel structure and properties of single and double nitrides. *Phys. Rev. B* **63**, 064102 (2001).
29. Sarmiento-Pérez, R., Cerqueira, T. F. T., Körbel, S., Botti, S. & Marques, M. A. L. Prediction of stable nitride perovskites. *Chem. Mater.* **27**, 5957–5963 (2015).
30. Hautier, G., Fischer, C., Ehrlacher, V., Jain, A. & Ceder, G. Data mined ionic substitutions for the discovery of new compounds. *Inorg. Chem.* **50**, 656–663 (2011).
31. Sun, W. et al. Thermodynamic routes to novel metastable nitrogen-rich nitrides. *Chem. Mater.* **29**, 6936–6946 (2017).
32. Ong, S. P. et al. Python materials genomics (pymatgen): a robust, open-source Python library for materials analysis. *Comp. Mater. Sci.* **68**, 314–319 (2013).
33. Jain, A. et al. Commentary: The Materials Project: a materials genome approach to accelerating materials innovation. *APL Mater.* **1**, 011002 (2013).
34. Kemp, C. & Tenenbaum, J. B. The discovery of structural form. *Proc. Natl Acad. Sci. USA* **105**, 10687–10692 (2008).
35. Johnson, S. C. Hierarchical clustering schemes. *Psychometrika* **32**, 241–254 (1967).
36. Gower, J. C. A general coefficient of similarity and some of its properties. *Biometrics* **27**, 857 (1971).
37. Pettifor, D. G. The structures of binary compounds. I. Phenomenological structure maps. *J. Phys. C: Solid State Phys.* **19**, 285–313 (1986).
38. Sun, W. et al. The thermodynamic scale of inorganic crystalline metastability. *Sci. Adv.* **2**, e1600225 (2016).
39. Bartel, C. J. et al. Physical descriptor for the Gibbs energy of inorganic crystalline solids and temperature-dependent materials chemistry. *Nat. Commun.* **9**, 4168 (2018).
40. Choi, J. & Gillan, E. G. Solvothermal metal azide decomposition routes to nanocrystalline metastable nickel, iron, and manganese nitrides. *Inorg. Chem.* **48**, 4470–4477 (2009).
41. Caskey, C. M., Richards, R. M., Ginley, D. S. & Zakutayev, A. Thin film synthesis and properties of copper nitride, a metastable semiconductor. *Mater. Horiz.* **1**, 424–430 (2014).
42. Bikowski, A. et al. Design of metastable tin titanium nitride semiconductor alloys. *Chem. Mater.* **29**, 6511–6517 (2017).
43. Arca, E. et al. Redox-mediated stabilization in zinc molybdenum nitrides. *J. Am. Chem. Soc.* **140**, 4293–4301 (2018).
44. Horvath-Bordon, E. et al. High-pressure chemistry of nitride-based materials. *Chem. Soc. Rev.* **35**, 987–1014 (2006).
45. Amsler, M., Hegde, V. I., Jacobsen, S. D. & Wolverton, C. Exploring the high-pressure materials genome. *Phys. Rev. X* **8**, 041021 (2018).
46. Yang, M. et al. Strong optical absorption in $CuTaN_2$ nitride delafossite. *Energy Environ. Sci.* **6**, 2994 (2013).
47. Aykol, M., Dwaraknath, S. S., Sun, W. & Persson, K. A. Thermodynamic limit for synthesis of metastable inorganic materials. *Sci. Adv.* **4**, eaaq0148 (2018).
48. Kuech, T. F., Babcock, S. E. & Mawst, L. Growth far from equilibrium: examples from III-V semiconductors. *Appl. Phys. Rev.* **3**, 040801 (2016).
49. Lambrecht, W. R. L. & Punya, A. in *III-Nitride Semiconductors and their Modern Devices* (ed. Gil, B.) 519–585 (Oxford Univ. Press, 2013).
50. Veal, T. D. et al. Band gap dependence on cation disorder in $ZnSnN_2$ solar absorber. *Adv. Energy Mater.* **5**, 1501462 (2015).
51. Anderson, W. P., Burdett, J. K. & Czech, P. T. What is the metallic bond? *J. Am. Chem. Soc.* **116**, 8808–8809 (1994).
52. Walsh, A., Sokol, A. A., Buckeridge, J., Scanlon, D. O. & Catlow, C. R. A. Oxidation states and ionicity. *Nat. Mater.* **17**, 958–964 (2018).
53. van Arkel, A. E. Molecules and crystals in inorganic chemistry. *J. Chem. Educ.* **34**, 417 (1957).
54. Etourneau, J., Portier, J. & Ménil, F. The role of the inductive effect in solid state chemistry: how the chemist can use it to modify both the structural and the physical properties of the materials. *J. Alloys Compd.* **188**, 1–7 (1992).

Acknowledgements

Funding for this study was provided by the US Department of Energy, Office of Science, Basic Energy Sciences, under contract no. UGA-0-41029-16/ER392000 as a part of the Department of Energy Energy Frontier Research Center for Next Generation of Materials Design: Incorporating Metastability. This research used resources of the Center for Functional Nanomaterials, which is a US Department of Energy Office of Science Facility, at Brookhaven National Laboratory under contract no. DE-SC0012704. This work also used computational resources sponsored by the Department of Energy's Office of Energy Efficiency and Renewable Energy, located at NREL. C.J.B. and A.M.H. acknowledge support in part from the Research Corporation for Science Advancement through the Scialog: Advanced Energy Storage award programme. Use of the Stanford Synchrotron Radiation Lightsource, SLAC National Accelerator Laboratory, is supported by the US Department of Energy, Office of Science, Office of Basic Energy Sciences under contract no. DE-AC02-76SF00515. W.S. thanks S. Y. Chan and N. U. Gulls for discussions and support.

Author contributions

W.S., B.O., A.M.H., S.L. and G.C. performed ternary nitride structure prediction; W.S., C.J.B., A.M.H. and S.L. computed phase stability; W.S. constructed the map; E.A., S.R.B., B.M., J.T., W.T. and A.Z. synthesized ternary nitride thin films; synchrotron XRD characterization was performed by B.-R.C., M.F.T. and L.T.S.; W.S., C.J.B., A.M.H. and G.C. performed the metallicity, ionicity and covalency analysis. W.S., C.J.B., A.M.H. and G.C. wrote the manuscript, with contributions and revisions from all authors.

Competing interests

The authors declare no competing interests.

Additional information

Supplementary information is available for this paper at https://doi.org/10.1038/s41563-019-0396-2.

Reprints and permissions information is available at www.nature.com/reprints.

Correspondence and requests for materials should be addressed to W.S. or A.M.H.

Publisher's note: Springer Nature remains neutral with regard to jurisdictional claims in published maps and institutional affiliations.

Methods

Ternary nitride structure prediction. Ternary nitride structures are generated using the data-mined structure prediction algorithm (DMSP) described in ref. [30]. Briefly, an ionic substitution matrix is trained on the ICSD, mapping isostructural compounds and identifying which cations are statistically likely to substitute for one another. In this work, the DMSP is trained on ionic substitutions in the pnictides (N + P + As + Sb), which is more predictive for nitride discovery than a substitution matrix trained over all inorganic solids—which otherwise becomes biased towards ionic substitutions that are common in the more thoroughly explored oxides and chalcogenides[31]. In general, substitution relationships in oxides are not applicable to nitrides because of differences in structure types, elemental coordination and metal redox chemistry for O^{2-} versus N^{3-} anions[55]. Training of the DMSP algorithm was performed on the ICSD as extracted in October 2015.

For the Zn–Mo–N, Zn–W–N, Zn–Sb–N, Mg–Ti–N, Mg–Zr–N, Mg–Hf–N and Mg–Nb–N systems, an unconstrained ground-state search was performed using the kinetically limited minimization approach[43], which does not require prototypical structures from databases. Details of the kinetically limited minimization approach can be found in Supplementary Section 4a. For each material, we sampled at least 100 seeds over the ternary compositions $A_iB_jN_k$ for ijk = 112, 146, 414, 213, 124, 326, 338 and 313, chosen to accommodate the $(Mg/Zn)^{2+}$, $M^{4+/5+/6+}$ and N^{3-} oxidation states.

Phase stability calculations. We calculated the total energies of the DMSP-suggested nitrides with DFT using the Vienna ab initio software package (VASP)[56,57], using the projector augmented-wave method with the Perdew–Burke–Ernzerhof exchange–correlation functional and projector augmented wave pseudopotentials. We used DFT basis cut-off energies and k-point densities in compliance with Materials Project calculation standards[58]. For each structure, we calculate ferromagnetic, ferrimagnetic and antiferromagnetic spin configurations, and choose the lowest-energy magnetic configuration for use in phase stability calculations.

Phase stability is computed using the convex hull phase diagram analysis package in Pymatgen[32]. Total energies of known nitride phases are retrieved from the Materials Project[33] using the Materials Project REST API[59]. Azides (for example NaN_3, WN_{18}) are removed from the phase diagram when computing phase stability, as these require non-typical solid-state synthesis techniques. Materials Project data were retrieved in January 2018.

Multifeature hierarchical clustering. We perform hierarchical clustering of the ternary nitrides using a multifeature distance matrix, based on the three features: formation energy, stability type (as indicated on the map as blue/green/red), and the periodic group in which the metal lies[36]. For each feature, we choose a distance metric that is best suited to the data type, and is scaled to fall between 0 and 1. For formation energy, which is continuous, we use the Euclidean distance. For stability type, which is a nominal data type, we use the Dice metric[60]. For periodic group, which is an ordinal data type, we use the Manhattan distance on columns as defined in the left-step periodic table[61]. The Gower distance, G, is a linear combination of the various distance matrices,

$$G_{M_1-M_2} = \sum_i W_i d^i_{M_1-M_2}$$

where W governs the weights of the various contributions[36]. We emphasize the clustering features with the following priority: formation energy of the stable compounds, formation energy of all compounds, chemical families, proximity of similar stability types (blue/green/red spaces) and white spaces (where the DMSP did not identify a reasonable compound substitution). Using the multifeature distance matrix between the various elements, we calculate the linkages using the 'average' method (UPGMA algorithm) and construct a dendrogram with optimal leaf ordering[62]. The branches are manually adjusted to order the elemental axes from left to right predominantly by stable (blue) → metastable versus binaries (green) → metastable versus elements (red). The resulting one-dimensional ordering of elements is set as the axis for the ternary nitride map. In Supplementary Section 2 we provide further details on the construction and clustering of the map, as well as a comparison with a ternary nitride map constructed from Pettifor's Mendeleev numbers[37].

Pressure-dependent stability. Using the approach developed by Amsler et al.[45], the enthalpy, H, of all compounds at a given pressure, p, is approximated by

$$H(p) = E_0 + \Delta pV(p_0)$$

where $p_0 = 0$ atm, E_0 is the DFT-calculated total energy at p_0, $\Delta p = p - p_0$, and $V(p_0)$ is the DFT-calculated volume per atom at $p = 0$. This enthalpy approximation is applied to all phases in each ternary phase diagram, with the exception of N_2, where the chemical potential is instead determined by accounting for the fugacity of supercritical N_2 as a function of pressure using the empirical reference data in ref. [44]. The stability of each ternary nitride was evaluated against all possible competing ternary, binary and elemental phases in the Materials Project using the resulting pressure-dependent enthalpies from 1 to 50 GPa. Entropic effects and pressure-dependent entropic effects are not accounted for in this pressure analysis. We did not consider ternary pernitrides (N_2^{4-})[63] or polynitrides (such as $N_3^{\delta-}$, $N_4^{\delta-}$, $N_5^{\delta-}$)[64–66] in this pressure analysis, due to lack of prototypes for the DMSP algorithm.

Synthesis and characterization. Experimental synthesis of Zn–Me–N and Mg–Me–N thin-film sample libraries was carried out by combinatorial radiofrequency magnetron sputtering using high-purity metal targets as cation sources. Ar and plasma-activated N_2 were used as sputtering gases. Before deposition, the sputtering chambers were evacuated to a pressure lower than 3×10^{-6} Torr. Cleaned Eagle-XG glass or fused silica slides were used as substrates, chosen specifically to avoid any crystalline substrate effects that could stabilize metastable phases through coherent epitaxial strains. Depositions were performed at a variety of pressures, gas flows, temperatures and sputtering powers to achieve the desired crystalline phases. Cation composition was determined by quantitative X-ray fluorescence. Sample points with exactly the same cation stoichiometry as the theoretically predicted compounds were subjected to high-resolution wide-angle X-ray scattering using the Stanford Synchrotron Radiation Lightsource Beamline 11–3. Further details on synthesis and characterization of Zn–Me–N and Mg–Me–N compounds can be found in Supplementary Section 4.

Metallicity, ionicity and covalency calculations. We compute ionicity from the charge density around each ion, calculated by taking the ratio of the stoichiometrically normalized net atomic charge over the summed bond order obtained from the density-derived electrostatic and chemical approach[67,68]. We use crystal orbital Hamiltonian population calculations as implemented in the LOBSTER code[69] to decompose the integrated bonding energies of metal–metal interactions (A–A, A–B, B–B) as metallicity, and non-metal interactions (A–N, B–N, N–N) as covalency. To compare Fermi energies and crystal orbital Hamilton population energy depths across a range of structures and compositions, we aligned energy levels from each Perdew–Burke–Ernzerhof calculation to core levels.

On the van Arkel triangle plots, the domain of metallicity, ionicity, covalency (M, I, C) is set by the maximum of each quantity within the dataset. For each phase, (M, I, C) is normalized such that the sum is equal to 1. Nitrogen excess or deficiency is compositionally referenced against the deepest-hull binary nitrides; for example, the formation of nitrogen-rich Ca_2VN_3 from Ca_3N_2 and VN requires excess nitrogen, whereas formation of nitrogen-poor Co_2Mo_3N from CoN and MoN requires nitrogen loss. To capture ion oxidation and reduction in a reaction from the deepest-hull binary nitrides to the stable ternary nitride, we cannot rely on formal oxidation states, which are often ambiguous to assign from DFT calculations[52]. Instead, we quantify the charge density around each ion i as the net atomic charge δ_i, and use the change in the net atomic charge between the deepest-hull binary nitrides and a ternary nitride, $\Delta\delta_i$, as a measure of ion oxidation or reduction. Further details of metallicity, ionicity and covalency calculations and analysis are discussed in Supplementary Section 7.

Data availability

We have made the structures and energies of the newly predicted nitrides freely available on the Materials Project (www.materialsproject.org) for readers interested in further investigation. All other data are available from the corresponding authors on request.

References

55. Gregory, D. H. Structural families in nitride chemistry. *J. Chem. Soc. Dalton Trans.* **1999**, 259–270 (1999).
56. Kresse, G. & Furthmüller, J. Efficient iterative schemes for ab initio total-energy calculations using a plane-wave basis set. *Phys. Rev. B* **54**, 11169–11186 (1996).
57. Kresse, G. & Furthmüller, J. Efficiency of ab-initio total energy calculations for metals and semiconductors using a plane-wave basis set. *Comp. Mater. Sci.* **6**, 15–50 (1996).
58. Jain, A. et al. A high-throughput infrastructure for density functional theory calculations. *Comp. Mater. Sci.* **50**, 2295–2310 (2011).
59. Ong, S. P. et al. The materials application programming interface (API): a simple, flexible and efficient API for materials data based on REpresentational State transfer (REST) principles. *Comp. Mater. Sci.* **97**, 209–215 (2015).
60. Dice, L. R. Measures of the amount of ecologic association between species. *Ecology* **26**, 297–302 (1945).
61. Scerri, E. R. in *The Periodic Table: Into the 21st Century* (eds Rouvray, D. and King, B.) 142–160 (Science Research, 2004).
62. Bar-Joseph, Z., Gifford, D. K. & Jaakkola, T. S. Fast optimal leaf ordering for hierarchical clustering. *Bioinformatics* **17**, S22–S29 (2001).
63. Bhadram, V. S., Kim, D. Y. & Strobel, T. A. High-pressure synthesis and characterization of incompressible titanium pernitride. *Chem. Mater.* **28**, 1616–1620 (2016).

64. Niwa, K. et al. Highly coordinated iron and cobalt nitrides synthesized at high pressures and high temperatures. *Inorg. Chem.* **56**, 6410–6418 (2017).
65. Yu, S. et al. Emergence of novel polynitrogen molecule-like species, covalent chains, and layers in magnesium–nitrogen Mg_xN_y phases under high pressure. *J. Phys. Chem. C* **121**, 11037–11046 (2017).
66. Bykov, M. et al. Fe-N system at high pressure reveals a compound featuring polymeric nitrogen chains. *Nat. Commun.* **9**, 2756 (2018).
67. Manz, T. A. & Limas, N. G. Introducing DDEC6 atomic population analysis: part 1. Charge partitioning theory and methodology. *RSC Adv.* **6**, 47771–47801 (2016).
68. Manz, T. A. Introducing DDEC6 atomic population analysis: part 3. Comprehensive method to compute bond orders. *RSC Adv.* **7**, 45552–45581 (2017).
69. Maintz, S., Deringer, V. L., Tchougréeff, A. L. & Dronskowski, R. LOBSTER: a tool to extract chemical bonding from plane-wave based DFT. *J. Comput. Chem.* **37**, 1030–1035 (2016).